THE ASTROPHYSICAL JOURNAL, 456:766–776, 1996 January 10

CORONA(E) OF AR LACERTAE. I. THE TEMPERATURE AND ABUNDANCE DISTRIBUTION

K. P. SINGH,[1,2,3] N. E. WHITE,[1,4] AND S. A. DRAKE[1,5,6]

Received 1995 April 24; accepted 1995 July 13

ABSTRACT

X-ray spectra of the RS CVn binary AR Lac, obtained from simultaneous observations with the *ROSAT* PSPC and the *ASCA* SIS and GIS detectors, have been analyzed to study the coronal temperature and abundance distribution. The spectra were jointly fitted with plasma emission models to the following possible temperature distributions: (*a*) one with discrete multitemperature emission components, (*b*) a continuous emission measure with a power-law dependence on temperature, and (*c*) a continuous emission distribution parameterized by the sum of a sixth-order Chebyshev polynomial. We find that (i) solar abundance plasma models with either discrete or continuous emission measure (CEM) distributions are rejected, (ii) the best fit is obtained with a two-temperature (2T) plasma emission model with an underabundance of the elements O, Mg, Si, S, Ar, Ca, and Fe by a factor of 3–4 relative to the solar photospheric values, and (iii) the best-fit CEM distribution also has similarly reduced abundances but fits the data less well than the 2T model. These results are confirmed even when the Fe-L region, which is subject to uncertainties in the atomic physics, is excluded from the fit. We consider optical depth effects as unlikely to be the explanation for the observed weakness of the line complexes relative to the continuum. Analysis of the spectral data during the primary and secondary eclipses shows that the emission measure of the high-temperature component in the 2T models appears to be more affected by the primary eclipse than the low-temperature component, suggesting that part of the former is concentrated in structures that are spatially more compact.

Subject headings: binaries: eclipsing — stars: abundances — stars: coronae — stars: individual (AR Lacertae) — X-rays: stars

1. INTRODUCTION

The most active late-type binaries are the RS CVn systems (Hall 1976), and these have been particularly well studied because they are the brightest coronal X-ray sources. The observed X-ray spectra of RS Canum Venaticorum–type binaries have often been fitted using thermal plasma models with two-temperature (2T) plasma components (Swank et al. 1981; Lemen et al. 1989; Dempsey et al. 1993; White et al. 1994). It has been debated whether the two components are an artifact produced by combining a more continuous temperature distribution with the low energy resolution, complex response, and limited bandwidth of the instruments used (e.g., Majer et al. 1986). Lemen et al. (1989) and Gehrels & Williams (1993) point out that in the absence of strong continuous heating in stellar coronae in which the energy balance is dictated by the radiative cooling, a bimodal temperature distribution occurs naturally from the condition of thermal stability of the plasma. The observed temperatures are in general agreement with the predictions of the plasma cooling curves. Considerable effort has been devoted (see Stern, Antiochos, & Harnden 1986; Schmitt et al. 1990; Ottmann 1993) to showing that a continuous distribution of temperatures can also fit the low-resolution data. The X-ray emission in these models comes from an ensemble of coronal loops with a single maximum temperature. The 2T model, however, has often given better fits to spectra of stellar coronae than the continuous emission measure models, either in cases with high-resolution spectra (Lemen et al. 1989) or in cases of low-resolution spectra with high signal-to-noise ratio (Dempsey et al. 1993).

The detection of very low elemental abundances in the corona of AR Lac and similar coronally active systems from moderate resolution X-ray spectroscopy using the *ASCA* (*Advanced Satellite for Cosmology and Astrophysics*) observatory (White et al. 1994; Antunes, Nagase, & White 1994; Drake et al. 1994; Singh, Drake, & White 1995) has further complicated the situation. Observation of a complete orbital cycle of AR Lac with the high-resolution detectors on the *ASCA* and a simultaneous observation with the *ROSAT* extends the energy bandwidth from 0.1 to 10 keV (White et al. 1994). These data provide an excellent opportunity to determine the emission measure temperature distribution for temperatures from 10^6 K to 10^8 K. A preliminary analysis of the spectral data from one of the two CCD detectors, SIS0, presented by White et al. (1994) indicates the line emission to be much weaker than predicted by a 2T solar abundance model. The direct interpretation of this result is that the abundances of the line producing elements (e.g., Fe, Si, S, etc.) are about one-third solar. White et al. (1994) show that the simultaneously obtained *ROSAT* spectrum of AR Lac also indicates reduced abundances, consistent with the *ASCA* result.

AR Lac is an RS Canum Venaticorum-type eclipsing binary with an orbital period of 1.98 days at a distance of 50 pc and is one of the brightest coronal X-ray sources. It contains a G2 IV primary with a radius of 1.54 $R_\odot$ and a cooler K0 IV secondary with a radius of 2.81 $R_\odot$ separated by 9.22 $R_\odot$. The X-ray luminosity is $\simeq 10^{31}$ ergs s^{-1}. From the recent *ROSAT* and *ASCA* observations, Ottmann, Schmitt, & Kurster (1993) and White et al. (1994) report an $\sim 50\%$ reduction in the X-ray flux during the primary eclipse and a shallow minimum near the

[1] Code 660, Laboratory for High Energy Astrophysics, NASA/Goddard Space Flight Center, Greenbelt, MD 20771.
[2] NRC-NASA Senior Research Associate, on leave from Tata Institute of Fundamental Research, Bombay, India.
[3] kps@rosserv.gsfc.nasa.gov.
[4] white@adhoc.gsfc.nasa.gov.
[5] Also USRA, Code 610.3, NASA/Goddard Space Flight Center.
[6] drake@lheavx.gsfc.nasa.gov.

time of the secondary eclipse, across the entire energy range observed.

In this paper, we present a joint reanalysis of the *ASCA* data taken during the off-eclipse phases and the simultaneously obtained *ROSAT* data to investigate the overall emission measure distribution in the corona of AR Lac, and to explore whether more complex emission measure distributions can explain the suppressed line emission. In addition, we have analyzed the *ASCA* spectra during the primary and secondary eclipses. A companion paper by Siarkowski et al. (1995) presents a map of the coronal structure of AR Lac based on a detailed modeling of the *ASCA* light curve in two energy bands.

The paper is organized as follows. In § 2 we present the details of observations, followed by the analysis and results in § 3. A discussion of all the results follows in § 4, before a summary of conclusions in § 5.

2. OBSERVATIONS

ASCA observed AR Lac from 1993 June 1 to June 3 as part of the performance verification program. A preliminary analysis of the observations has been presented by White et al. (1994), and the *ASCA* light curves from the SIS and GIS detectors are shown in Figure 1 of that paper. A description of *ASCA* is given in Tanaka, Inoue, & Holt (1994). In brief, *ASCA* has two Solid State Imaging Spectrometers (SIS0 and SIS1; Burke et al. 1991), each with four CCD chips, and two Gas Imaging Spectrometers (GIS2 and GIS3; Ohashi et al. 1991), each at the focus of imaging telescopes (Serlemitsos et al. 1995). The energy resolution of both SISs is about 2% (FWHM) at 5.9 keV, degrading to 6% at 1.0 keV. The energy resolution of the GISs is about 7.8% (FWHM) at 5.9 keV and 19% at 1.0 keV. The energy bandwidth for greater than 10% efficiency is 0.5–10 keV for the SISs and 0.8–10 keV for the GISs. The data were selected as described by White et al. (1994), but with the additional constraint that data taken during satellite passage through regions with geomagnetic rigidity less than 6 GeV per count for SIS (<7 GeV per count for GIS) detectors were not accepted. The counts and pulse height spectra were accumulated separately for the times when AR Lac was (*a*) out of any eclipse (exposure time = 47,464 s), (*b*) undergoing the primary eclipse (exposure time = 8823 s), and (*c*) in secondary eclipse (exposure time = 6341 s). The spectra were accumulated for these times from a source region of 4′ radius in the SIS and 6′ radius in the GIS, while the background was taken from source-free regions in the SIS and GIS. The spectral data were grouped so that there were at least 20 counts per pulse height bin.

AR Lac was observed with *ROSAT* as a part of the *ROSAT* guest observer program, simultaneously with *ASCA*. The observations were done with the *ROSAT* X-ray telescope and a position sensitive proportional counter (PSPC) as the detector (Trümper 1983; Pfeffermann et al. 1987). The PSPC has an energy resolution ($\Delta E/E$) of $\simeq 0.42$ at 1 keV and a bandwidth of 0.1–2.4 keV. The spectral resolution is quite moderate when compared with that of the *ASCA* detectors, but the lower energy range is more sensitive to the presence of soft emission components. A preliminary analysis of the PSPC spectrum showing its consistency with the *ASCA* spectrum was presented earlier by White et al. (1994). The *ROSAT* observations have a total duration of 5414 s, with 4039 s overlapping with *ASCA*. This was when AR Lac was not undergoing any eclipses, and at binary phases 0.22, 0.69, 0.76, and 0.79. The rest of the *ROSAT* observations preceded the *ASCA* observations and were on the previous binary cycle at phase 0.60 and at a similar count rate to the overlapping observation. The source counts were selected from a radius of about 4′.0. The background was accumulated from several neighboring source-free regions. No time variability was detected during the *ROSAT* observations, and the spectra from the entire PSPC observations were accumulated for a total exposure time of 4900 s after screening for high background events and data dropouts. This resulted in a very good quality spectrum with a total of 26,116 counts. The pulse height data were grouped so as to have at least 20 counts per pulse height bin. The data in the last 18 pulse height bins (239–256) were ignored because of very low counts.

3. ANALYSIS AND RESULTS

The problem of inferring the temperature distribution of a thermal X-ray source from its spectrum was discussed formally by Craig & Brown (1976). They pointed out that because of the exponential nature of emissivity as a function of temperature involved in each of the basic processes (bremsstrahlung, recombination, and line emission), photons of a certain energy cannot be closely identified with plasma at a precise temperature in the source, and that any procedure for inverting the spectral data to infer emission measure distribution in a source magnifies observational errors. They showed that the problem is not easily simplified by simply having a very high spectral resolution; instead, a large bandwidth and very high signal-to-noise ratio can be equally if not more important for this problem. The energy resolution of the *ASCA* detectors is not sufficient to infer the temperature structure from the inversion of the line ratios. The large 0.4–10.0 keV bandwidth is, however, very valuable in testing for the presence of high-temperature components and in determining the relative strength of the line complexes with respect to the continuum. The use of simultaneously obtained *ROSAT* data can extend the bandwidth so that nearly two decades (0.1–10.0 keV) of energy range are covered. Swartz et al. (1994) have addressed the problem of inferring temperatures from X-ray spectra with specific regard to *ASCA* SIS spectra. They showed that temperatures derived from line ratios can only cover a narrow range of temperature, and that the best statistical precision is obtained by fitting the entire spectrum. In our analysis below, this is the strategy that we follow. We use the χ^2 minimizing criterion to search for the best-fitting spectral model from a number of competing models with differing temperature distributions that have been proposed in previous studies.

3.1. *Spectral Analysis: Models*

We have used the XSPEC (version 8.50) spectral analysis package to fit the data with the spectral models for thermal equilibrium plasma known as the Mewe-Kaastra, or "meka," model (Mewe, Gronenschild, & van den Oord 1985; Kaastra 1992). Another spectral model for thermal plasmas, called the Raymond & Smith or RS model (Raymond 1990; Raymond & Smith 1977), was also tried. Except for a small difference in the derived temperatures, the two spectral models give similar results. The results presented here are based on the "meka" model for ease of comparison with our earlier work on late-type stars, in which we also found somewhat better fits using the "meka" model (White et al. 1994; Drake et al. 1994). We have tried (*a*) single-temperature or isothermal plasma models, (*b*) a model consisting of two or more discrete plasma components at different temperatures, (*c*) a plasma model with

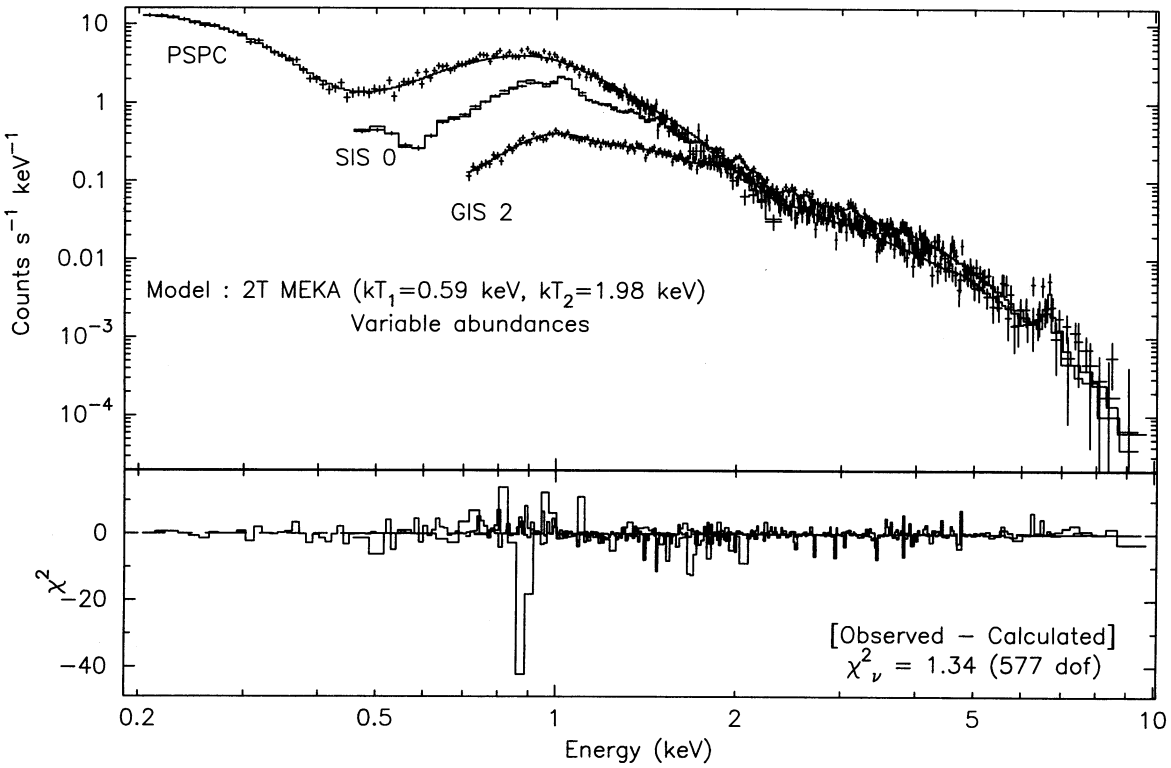

FIG. 1*a*

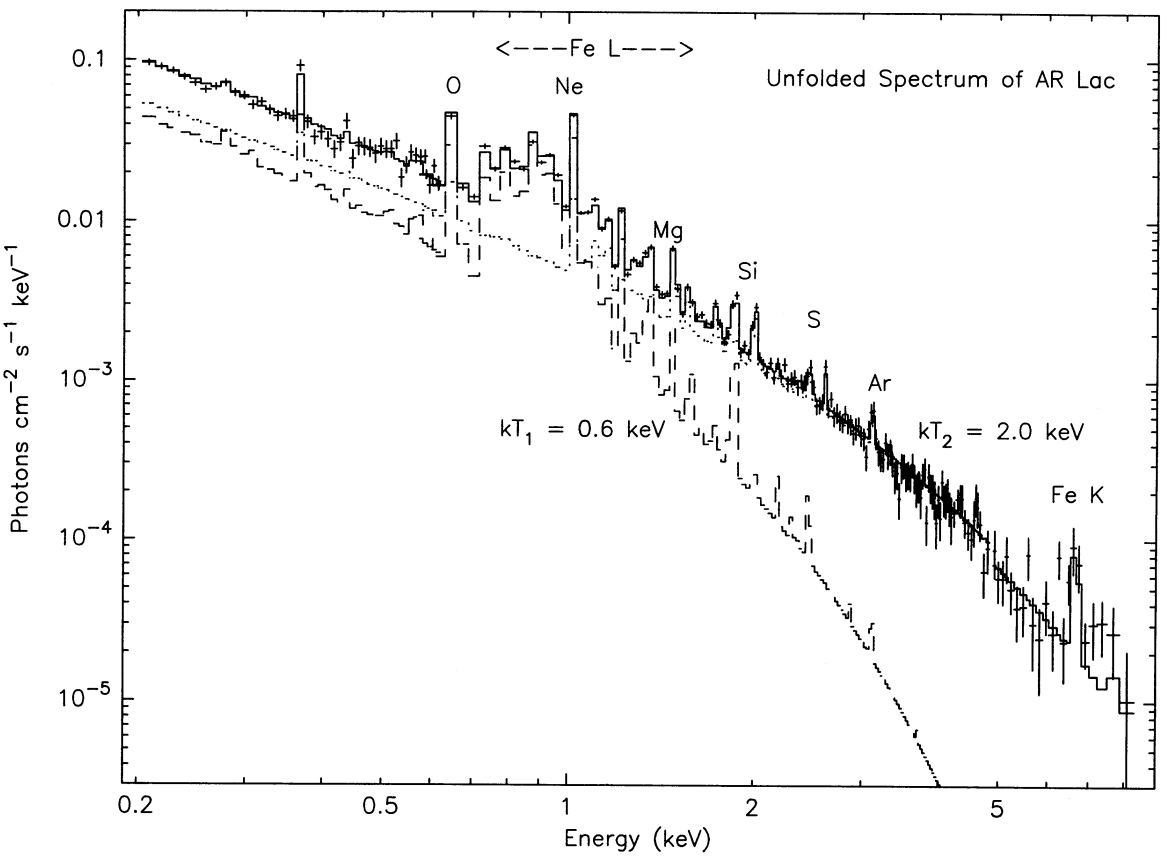

FIG. 1*b*

FIG. 1.—(*a*) X-ray spectra of AR Lac as observed with the SIS0 and GIS2 detectors aboard *ASCA* and the PSPC detector aboard *ROSAT*. The best-fit two-component model jointly fitted to the three spectra are shown as histograms. The lower panel shows the contribution of the residuals to the χ^2. (*b*) The unfolded X-ray–incident X-ray spectrum showing the contributions of the two components. Note that the 2 keV component dominates over the entire bandwidth. The elements responsible for the prominent lines in the spectrum are marked in the figure. The lines indicated to be from O and Ne are from highly ionized H-like ions of these elements, those from Mg, Si, S, and Ar are from both H-like and He-like ions, and the Fe K line is from He-like ions.

continuous emission measure (CEM) distribution which is a power-law function of the temperature of the type $EM(T) \propto (T/T_{max})^{\alpha}$, where the maximum temperature of the plasma, T_{max}, and the slope of the emission, α, are treated as free parameters (Schmitt et al. 1990) (hereafter referred to as CPL), and (*d*) a CEM plasma model parameterized by the exponential of a sum of terms of an *n*th-order Chebyshev polynomial in the log EM–log T plane (see Lemen et al. 1989 for details) (henceforth referred to as CCP). The CEM distributions and the plasma emissivity functions were integrated over steps of 0.05 in log T in the case of CPL and over steps of 0.1 in the case of CCP. The range of integration for CCP was from 5.8 to 8.0 in log T. For CCP models, we tried polynomials from third to sixth order. Since the number of free parameters increases in going to higher orders, we adopted the sixth-order polynomial as describing a reasonably complex distribution with optimum number of variable parameters, and for ease of computation. The elemental abundances in the plasma for all these different models could be varied with respect to the solar photospheric values taken from Anders & Grevesse (1989). The solar photospheric abundances of the elements considered are listed here in number units in which the $\log_{10}$ abundance of H is fixed at 12. These are 10.99, 8.56, 8.05, 8.93, 8.09, 6.33, 7.58, 6.47, 7.55, 7.21, 6.56, 6.36, 7.67, and 6.25 for He, C, N, O, Ne, Na, Mg, Al, Si, S, Ar, Ca, Fe, and Ni, respectively.[7]

The CPL and CCP models are an approximation that describe the EM distribution of static coronal loops on the sun (Vesecky, Antiochos, & Underwood 1979; Antiochos & Noci 1986). Although it is not clear at present whether these models are applicable to RS CVn stars like AR Lac, whose coronae are much hotter and very much more X-ray–luminous than the Sun (see § 4 below), these models have been used to fit the X-ray emission from stellar coronae which would normally involve an ensemble of such loops (Lemen et al. 1989; Schmitt et al. 1990; Dempsey et al. 1993). Most recently, the CCP models (which are probably a more accurate representation of the actual coronal loops than CPL) have been used in the analysis of extreme-ultraviolet (EUV) spectra of the coronae of active stars (Stern et al. 1995). More complex coronal loop models have been used by Stern et al. (1986) and Ottmann (1993). The integration of emissivity in these loops assumes piecewise power-law approximations to the radiative loss function (Vesecky et al. 1979). The resultant distribution of EM shows a minimum near log $T = 5.5$ K, a power law above it, and a sharp increase near T_{max}. The slope of the power-law component depends on the expansion factor of the loops, becoming steeper for larger expansion factors. The flattening of the EM distribution is at sufficiently low temperatures that the X-ray emission is below the energy range in our spectra. The advantage of such models is that they provide an interpretation based on a well-studied analog of static solar loops. For interactive fitting, the calculations of these models are complicated and require an enormous amount of computer time. Instead, loop emissivities are tabulated in a four-dimensional space corresponding to the four most interesting free parameters, namely, T_{max}, loop expansion parameter, loop size, and the filling factor. The best fit is then ascertained by testing all possible combinations or by interpolation in four-dimensional space. This becomes increasingly difficult if elemental abundances are nonsolar, requiring an additional parameter for each element. On the other hand, a formal empirical treatment with a specific EM distribution function has certain advantages. For example, it is easier to convolve numerically with realistic plasma cooling functions, which is important while using medium- to high-resolution data as the contributions from different elements may need to be varied, thus also changing the cooling curve. As we will see later, *ASCA* data are particularly sensitive with regard to elemental abundances.

Recent experimental and analytical X-ray spectroscopic studies have shown the shortcomings of the atomic physics in the present plasma codes, which are particularly evident in the 0.7–1.5 keV energy range (Liedahl, Osterheld, & Goldstein 1995). The effect is mostly concentrated around the Fe-L emission-line complexes near 0.9 keV and 1.3 keV and is mostly confined to temperature components below 2 keV. To avoid the uncertainties in the plasma codes in this energy range, we have (in addition to our analysis of the complete 0.2–9.0 keV spectral range) also analyzed the spectra with the 0.7–1.7 keV energy range excluded.

3.2. *Joint Analysis of PSPC, SIS0, and GIS2 X-Ray Spectra*

3.2.1. 0.2–9.0 keV *Spectra*

The background-subtracted spectral data from the PSPC, and from SIS and GIS during the off-eclipse phases, were analyzed jointly using the above spectral models. The relative normalizations of the models were kept as independent parameters for all the detectors. For the PSPC data, we used the appropriate PSPC response matrix available, *pspcb_93jan12.rmf* (Turner & George 1994). Owing to some calibration uncertainties in the response function of the PSPC at very low energies, we have ignored the data in the first 19 pulse height channels and include only the data above 0.19 keV. During the joint fitting, it was found that a small reduction (4%) in the slope of the energy–to–pulse height channel relation or the gain of the PSPC improved the fit considerably. Such a gain shift in the PSPC is allowed, as small drifts in the calibration of the PSPC are not corrected for in the response matrix used (see Turner & George 1994). For the SISs and GISs, we used the latest energy redistribution matrices available as of 1995 March 7 (version 0.8 for the SISs and version 4.0 for the GISs) and used the effective area curves corrected for the position of the source and the accumulation region. Data in a few pulse height channels in the beginning and in the end in the SIS and GIS spectra containing very few counts in them were ignored while fitting the data. For the joint fit with the PSPC, we present the results from the analysis, taking SIS0 and GIS2 into consideration for the purpose of clarity. The SIS1 data were consistent with SIS0, and similarly the GIS3 data were consistent with the GIS2, in the sense that the best fits with the common spectral model resulted in the same normalization factor for these pairs of detectors.

The solar abundance plasma models with two-temperature (2T), three-temperature (3T), or four-temperature (4T) components were found to be poor fits to the spectra with the minimum reduced χ^2 (hereafter χ^2_ν) being 3.66 (for 589 degrees of freedom) for 2T, 2.40 (for 587 degrees of freedom) for 3T, and 2.40 (for 585 degrees of freedom) for 4T components. A significantly better fit was found for the two-component spectral

[7] In a revision of the solar photospheric abundance values suggested by Grevesse, Noels, & Sauval (1992), the values of N, O, and Fe have been changed to 7.97, 8.87, and 7.51, respectively. The effect of this revision on our results would be to scale the derived values of N, O, and Fe by factors of 1.20, 1.15, and 1.44, respectively.

TABLE 1

SPECTRAL RESULTS FOR TWO-TEMPERATURE "MEKA" MODEL: OFF-ECLIPSE PSPC, SIS0, AND GIS2 DATA

A. MODEL PARAMETERS

Parameter	Total Energy Range	Excluding 0.7–1.7 keV Region
N_H (10^{18} cm^{-2})	<4.4	<6.0
kT_1 (keV)	$0.586^{+0.014}_{-0.016}$	$0.60^{+0.035}_{-0.035}$
EM_1 (10^{53} cm^{-3})	$4.14^{+0.27}_{-0.27}$	$4.2^{+0.6}_{-0.6}$
kT_2 (keV)	$1.98^{+0.05}_{-0.06}$	$2.0^{+0.1}_{-0.1}$
EM_2 (10^{53} cm^{-3})	$6.25^{+0.23}_{-0.25}$	$6.0^{+0.4}_{-0.5}$
χ^2_ν/Degrees of freedom	1.336/577	0.954/364

B. ABUNDANCES RELATIVE TO SOLAR PHOTOSPHERIC VALUES

Element	Total Energy Range	Excluding 0.7–1.7 keV Region
N	<0.15	<0.27
O	$0.41^{+0.05}_{-0.04}$	$0.44^{+0.09}_{-0.09}$
Ne	$1.42^{+0.13}_{-0.13}$	1.0(f)
Mg	$0.50^{+0.07}_{-0.07}$	1.0(f)
Si	$0.40^{+0.06}_{-0.06}$	$0.47^{+0.08}_{-0.07}$
S	$0.19^{+0.09}_{-0.09}$	$0.26^{+0.09}_{-0.11}$
Ar	$0.31^{+0.27}_{-0.27}$	$0.49^{+0.25}_{-0.33}$
Ca	<0.25	<0.47
Fe	$0.29^{+0.02}_{-0.03}$	$0.47^{+0.10}_{-0.09}$
Ni	$1.14^{+0.41}_{-0.30}$	1.0(f)

C. RELATIVE NORMALIZATIONS FOR THE MODEL IN DIFFERENT DETECTORS

Detector Name	Total Energy Range	Excluding 0.7–1.7 keV Region
PSPC	1.0(f)	1.0(f)
SIS0	$0.95^{+0.01}_{-0.02}$	0.95(f)
GIS2	$0.77^{+0.02}_{-0.01}$	0.77(f)

NOTE.—Errors and upper limits are with 90% confidence based on $\chi^2_{min} + 2.71$; f means frozen value.

model with *nonsolar abundances* for the elements N, O, Ne, Mg, Si, S, Ar, Ca, Fe, and Ni. The values for the best-fit parameters with their uncertainties are given in Table 1. The χ^2_ν is 1.34 for 577 degrees of freedom. The detector normalization values represent a multiplicative constant for the normalization of the common models fitted to data from a detector for a joint fit. The best-fit model and the data are shown in Figure 1*a* along with the residual χ^2 multiplied by the sign of the difference between the observed data and the calculated model. These results are consistent with those reported by White et al. (1994) based on a single SIS0 spectrum. In addition, we derive a limit on the equivalent column density of hydrogen in the line of sight to AR Lac of $<4.4 \times 10^{18}$ cm^{-2}. This compares very well with the estimates obtained from nearby stars at about the same distance as AR Lac, 10^{18} cm^{-2} for κ And, 2.5×10^{18} cm^{-2} for α Lac, and $(4.0–20.0) \times 10^{18}$ cm^{-2} for the white dwarf WD 2111+498 (Diplas & Savage 1994; Fruscione et al. 1994). The incident two-component spectrum is shown in Figure 1*b*. The emission from the 2 keV component dominates the entire bandwidth except for a small region near the O and Fe-L emission-line complex. The Fe-L line emission comes almost entirely from the 0.6 keV component.

The CPL model with solar photospheric abundances, $\alpha = 2.1$ and $T_{max} = 2.73$ keV, gave a best fit with $\chi^2_\nu = 4.61$ for 588 degrees of freedom. The best-fit model and the data are displayed in Figure 2*a* and show the inadequacy of this model to fit the data over the large bandwidth and the high resolution of the *ASCA* detectors. Varying the abundances of N, O, Ne, Mg, Si, S, Ar, Ca, Fe, and Ni individually in the CPL model improved the fit considerably with $\chi^2_\nu = 1.77$ for 578 degrees of freedom. The best-fit values for α and T_{max} are 1.67 and 3.4 keV, respectively. The best-fit values of the other parameters and their uncertainties are given in Table 2. The best-fit model and the data are plotted in Figure 2*b* along with the residual χ^2 as in Figure 1*a*. A comparison with Figure 1*a* shows that the fit looks fairly similar even though, statistically, it is considerably poorer than the 2T variable abundance model with $\Delta\chi^2 = 248$. Based on the *F* statistic, the CPL model has a probability of only 0.0005 of providing a fit which is as good as that with the 2T model. The CCP model based on the sixth-order polynomial and assuming solar abundances gave a $\chi^2_\nu = 5.2$, even worse than the corresponding fit with the CPL. The CCP model with nonsolar abundances gives a better fit with $\chi^2_\nu = 1.54$ for 573 degrees of freedom. It is, however, still worse than the 2T nonsolar fit, as reflected in the $\Delta\chi^2$ value of 108. The CCP model has about a 3.5% chance of providing a fit which is as good as that with the 2T model, on the basis of the *F* statistic. The best fit with the CCP model is shown in Figure 2*c*, and the parameter values are listed in Table 3. The tem-

TABLE 2

SPECTRAL RESULTS FOR CPL MODEL: OFF-ECLIPSE PSPC, SIS0, AND GIS2 DATA

A. MODEL PARAMETERS

Parameter	Total Energy Range	Excluding 0.7–1.7 keV Data
kT_{max} (keV)	$3.4^{+0.15}_{-0.15}$	$3.06^{+0.18}_{-0.18}$
Slope (α)	$1.66^{+0.04}_{-0.03}$	$2.05^{+0.06}_{-0.06}$
N_H (10^{18} cm^{-2})	30^{+6}_{-7}	<9
χ^2_ν/Degrees of freedom	1.77/578	1.13/365

B. ABUNDANCES RELATIVE TO SOLAR PHOTOSPHERIC VALUES

Element	Total Energy Range	Excluding 0.7–1.7 keV Data
N	<0.20	<0.20
O	$0.34^{+0.05}_{-0.05}$	$0.53^{+0.07}_{-0.07}$
Ne	$2.0^{+0.16}_{-0.14}$	1.0(f)
Mg	$0.72^{+0.12}_{-0.12}$	1.0(f)
Si	$0.58^{+0.08}_{-0.08}$	$0.55^{+0.08}_{-0.08}$
S	$0.23^{+0.11}_{-0.11}$	$0.27^{+0.1}_{-0.1}$
Ar	<0.35	$0.45^{+0.3}_{-0.3}$
Ca	<0.30	<0.44
Fe	$0.37^{+0.03}_{-0.03}$	$0.48^{+0.05}_{-0.05}$
Ni	$2.8^{+1.0}_{-0.4}$	$4.6^{+2.0}_{-2.0}$

C. RELATIVE NORMALIZATIONS IN DIFFERENT DETECTORS

Detector Name	Total Energy Range	Excluding 0.7–1.7 keV Data
PSPC	1.0(f)	1.0(f)
SIS0	$1.0^{+0.01}_{-0.02}$	1.0(f)
GIS2	$0.83^{+0.02}_{-0.02}$	0.83(f)

NOTE.—Errors and upper limits are with 90% confidence based on $\chi^2_{min} + 2.71$; f means frozen value.

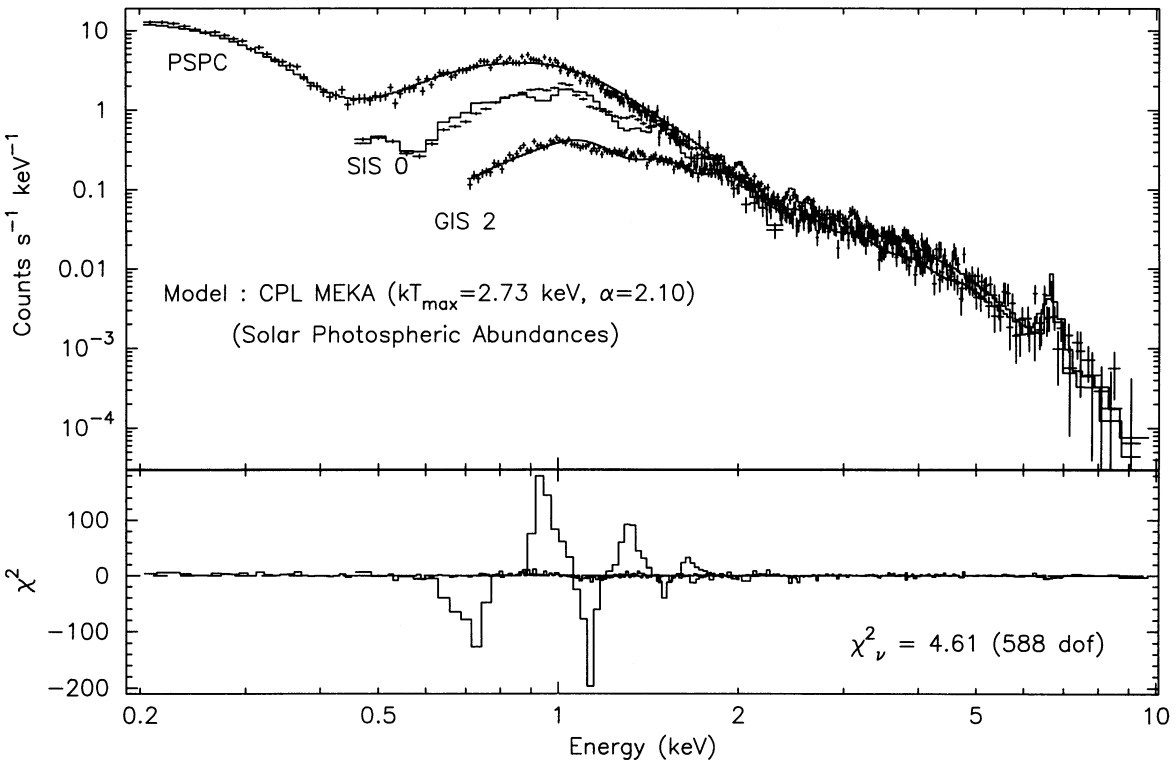

FIG. 2*a*

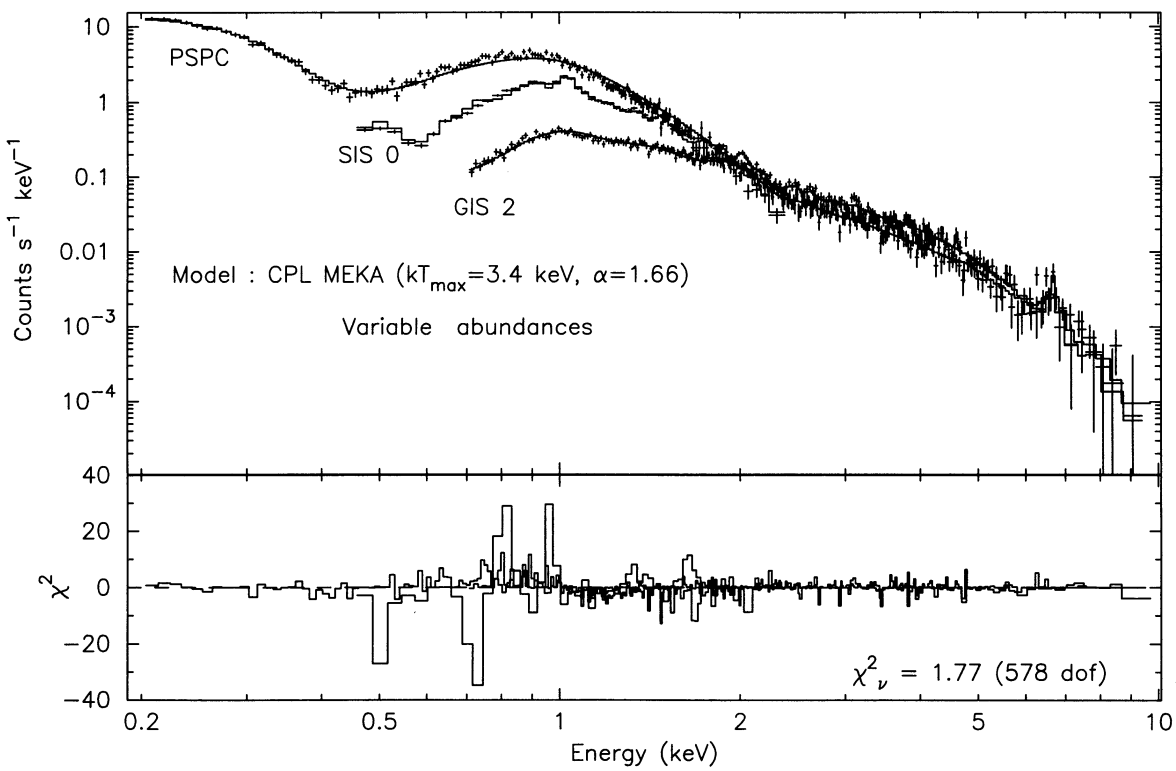

FIG. 2*b*

FIG. 2.—(*a*) Same as Fig. 1*a* for the CPL model with solar photospheric abundances. (*b*) Same as (*a*) for nonsolar photospheric abundances. (*c*) Same as Fig. 1*a* for the CCP (sixth-order Chebyshev polynomial) model with nonsolar photospheric abundances.

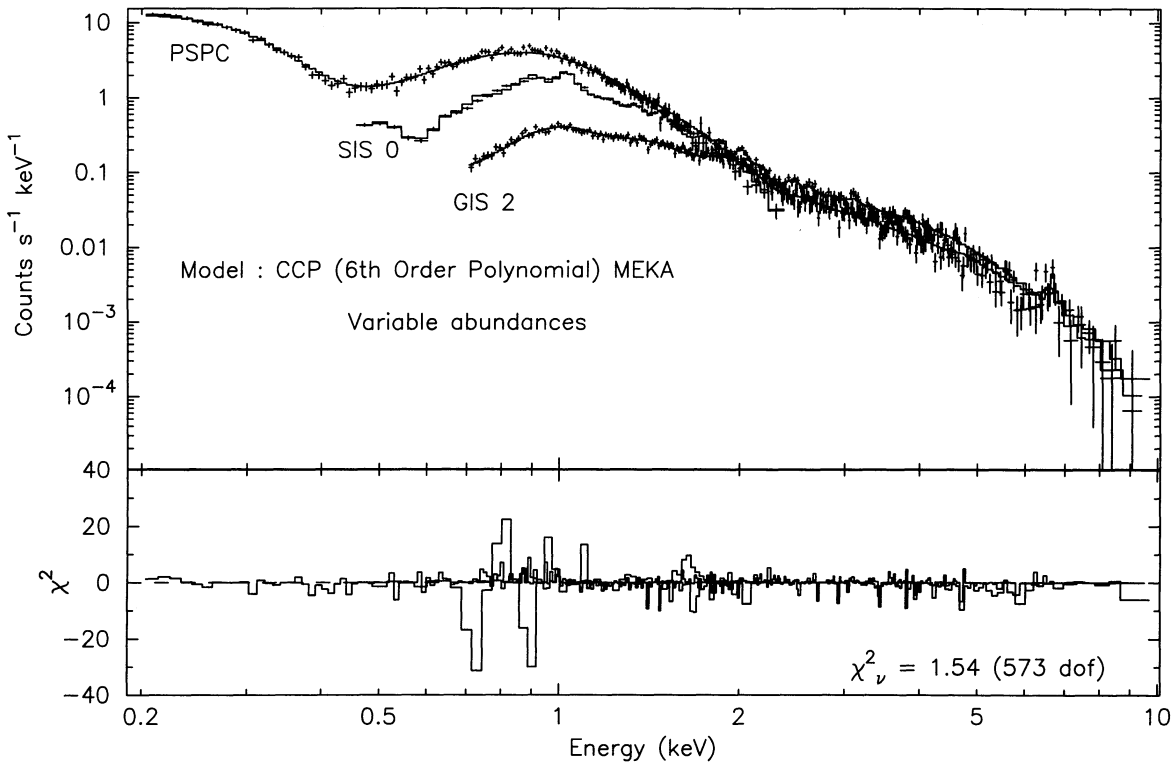

FIG. 2c

TABLE 3

SPECTRAL RESULTS FOR CCP MODEL: OFF-ECLIPSE PSPC, SIS0, AND GIS2 DATA

A. MODEL PARAMETERS

Parameter	Total Energy Range	Excluding 0.7–1.7 keV Data
N_H (10^{18} cm^{-2})	32 ± 7	41 ± 10
χ^2_ν/Degrees of freedom	1.54/573	1.13/360

B. ABUNDANCES RELATIVE TO SOLAR PHOTOSPHERIC VALUES

Element	Total Energy Range	Excluding 0.7–1.7 keV Data
N	<0.20	<0.20
O	$0.24^{+0.05}_{-0.05}$	$0.26^{+0.07}_{-0.07}$
Ne	$1.37^{+0.17}_{-0.15}$	1.0(f)
Mg	$0.66^{+0.11}_{-0.11}$	1.0(f)
Si	$0.47^{+0.07}_{-0.07}$	$0.51^{+0.07}_{-0.07}$
S	$0.25^{+0.11}_{-0.11}$	$0.33^{+0.1}_{-0.1}$
Ar	<0.5	$0.47^{+0.2}_{-0.3}$
Ca	<0.3	<0.5
Fe	$0.25^{+0.03}_{-0.03}$	$0.19^{+0.05}_{-0.05}$
Ni	$2.2^{+1.0}_{-0.4}$	$5.3^{+2.0}_{-2.0}$

C. RELATIVE NORMALIZATIONS IN DIFFERENT DETECTORS

Detector Name	Total Energy Range	Excluding 0.7–1.7 keV Data
PSPC	1.0(f)	1.0(f)
SIS0	$0.95^{+0.02}_{-0.02}$	0.95(f)
GIS2	$0.78^{+0.02}_{-0.02}$	0.78(f)

NOTE.—Errors and upper limits are with 90% confidence based on $\chi^2_{min} + 2.71$; f means frozen value.

perature distribution of the EM in this model is shown in Figure 3, where we plot the 90% confidence limits corresponding to $\chi^2_{min} + 10.6$, for six coefficients of interest, and assuming the abundances fixed at their values given in Table 3. The actual range of distribution in Figure 3, for all variable parameters, would be larger than shown. For comparison, we show in Figure 3 the emission measure distribution from the best-fit CPL model. The values of the total EMs of the best-fit 2T components plotted in Figure 3 are for showing their relative

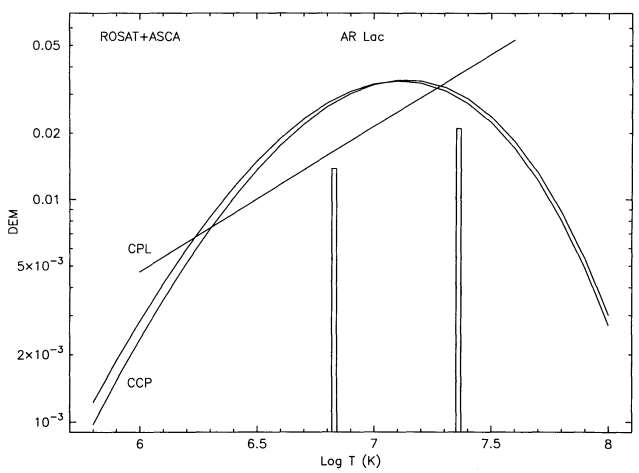

FIG. 3.—The differential emission measure distribution for the best-fit variable abundance CPL model, and the variable abundance CCP model based on the allowed range for the uncertainty in the six polynomial coefficients keeping the abundances fixed at their nonsolar values in Table 3. The EM is plotted in units of 3×10^{55} cm^{-3}. The total emission measures of the best-fit 2T components plotted are only indicative of the relative strength of the two components.

strengths only. Both the CEM models require an implausibly large value for the N_H of 20–40 $\times$ 10^{18} cm^{-2} toward AR Lac.

From the best-fit relative normalizations it is found that, irrespective of the models used, the current GIS response matrices overpredict the X-ray flux by 15%–19% with respect to the flux in the SIS detectors, requiring a scaling down of the normalization for the GIS detectors for a given model fitted to the SIS detectors (Tables 1–4). The PSPC, however, requires very little correction to match the flux in the SIS detectors.

3.2.2. *Excluding the* 0.7–1.7 keV *Data*

A comparison of the residuals in Figures 2*b* and 2*c* with Figure 1*a* shows that the major contribution to the difference in the χ^2 comes from very low energy data points and the region near 1 keV in which the plasma codes are suspect. We have, therefore, further explored the modeling of the spectra by ignoring the region between 0.7–1.7 keV. Since the spectra are well determined at low and high energies, excluding this region is not expected to affect the results on the continua and the contribution to line emission outside the region. We repeated all the model fits in the previous section to verify here how sharply our previous results were influenced by the Fe-L emission region. Solar abundance models with 2T, 3T, and 4T components gave $\chi^2_\nu = 2.4$ (371 degrees of freedom), $\chi^2_\nu = 1.29$ (369 degrees of freedom), and 1.29 (367 degrees of freedom), respectively. The best fit is still the 2T variable abundance plasma model with a $\chi^2_\nu = 0.95$ for 364 degrees of freedom, and subsolar abundances of N, O, Si, S, Ar, Ca, and Fe. The data are no longer sensitive to the abundances of Ne and Mg, since their dominant line features lie in the spectral region that we have excluded. The results were also insensitive to the abundance of Ni. The best-fit parameter values with their uncertainties are listed in Table 1. The temperatures, emission measures, and even the abundances of the most elements are hardly affected at all when compared to the analysis based on the complete data (see previous section). This indicates that the values of coronal abundances derived for O, Si, S, Ar, and Ca are quite robust. The coronal abundance value derived for Fe is now based entirely on the strength of the Fe K line emission, which has poorer statistical quality. The Fe abundance derived here confirms a subsolar value. The value of $\simeq$0.5 solar is slightly higher than the value of $\simeq$0.3 obtained when the entire spectrum is considered.

The CPL and CCP models with solar photospheric abundances give a poorer fit, with $\chi^2_\nu \geq 2$ for 372 and 367 degrees of freedom, respectively. The best-fit values for α and T_{max} in the CPL model are 2.24 and 3.05 keV, respectively. Both the CEM models with nonsolar abundances gave an equally good fit with $\chi^2_\nu = 1.13$ for 365 and 360 degrees of freedom, respectively. The best-fit values for α and T_{max}, in the case of the CPL model, are 2.05 and 3.06 keV, respectively. The best-fit parameter values for the CPL model are given in Table 2, and those of the CCP model are given in Table 3 along with their uncertainties. The derived value of N_H based on the CPL model is now consistent with the low values derived using the 2T models, although the CCP model still gives a higher value for N_H. The CCP model also gives lower abundances for O and Fe compared to the other models. Apart from the abundance of these two elements, the abundances of other elements are almost independent of the model used. The low abundance of Fe is very likely the result of the presence of hotter plasmas in the CCP model which produce the Fe emission more efficiently. Although the CEM models with nonsolar abundances give an acceptable fit, the fit is somewhat poorer than the 2T nonsolar model, as the difference of $\geq$59 in the minimum χ^2 suggests. The probability of the 2T model being better than the CEM models is 87%–95%, based on the *F* statistic. Nevertheless, the low values of the abundances derived for most of the elements in the coronal plasma of AR Lac appear to be independent of the assumed temperature distribution.

TABLE 4

SPECTRAL RESULTS FOR TWO-TEMPERATURE "MEKA" MODEL BASED ON ALL FOUR *ASCA* DETECTORS

A. MODEL PARAMETERS

Parameter	Off-Eclipse	Primary Eclipse	Secondary Eclipse
N_H (10^{18} cm^{-2})	4.4(f)	4.4(f)	4.4(f)
kT_1 (keV)	$0.60^{+0.01}_{-0.01}$	$0.59^{+0.01}_{-0.02}$	$0.59^{+0.01}_{-0.02}$
EM_1 (10^{53} cm^{-3})	$4.64^{+0.3}_{-0.2}$	$3.0^{+0.2}_{-0.2}$	$4.1^{+0.3}_{-0.3}$
kT_2 (keV)	$2.04^{+0.04}_{-0.05}$	$1.95^{+0.16}_{-0.14}$	$1.89^{+0.15}_{-0.13}$
EM_2 (10^{53} cm^{-3})	$5.60^{+0.2}_{-0.1}$	$3.1^{+0.3}_{-0.2}$	$4.8^{+0.3}_{-0.4}$
χ^2_ν/Degrees of freedom	1.400/800	0.92/345	0.905/362

B. ABUNDANCES RELATIVE TO SOLAR PHOTOSPHERIC VALUES

Element	Off-Eclipse	Primary Eclipse	Secondary Eclipse
N	<0.10	0.0(f)	0.0(f)
O	$0.36^{+0.04}_{-0.03}$	0.36(f)	0.36(f)
Ne	$1.18^{+0.1}_{-0.1}$	1.18(f)	1.18(f)
Mg	$0.47^{+0.05}_{-0.05}$	0.47(f)	0.47(f)
Si	$0.43^{+0.04}_{-0.04}$	0.43(f)	0.43(f)
S	$0.24^{+0.06}_{-0.06}$	0.24(f)	0.24(f)
Ar	$0.32^{+0.19}_{-0.19}$	0.32(f)	0.32(f)
Ca	<0.26	0.0(f)	0.0(f)
Fe	$0.26^{+0.02}_{-0.02}$	0.26(f)	0.26(f)
Ni	$1.02^{+0.2}_{-0.2}$	1.02(f)	1.02(f)

C. RELATIVE NORMALIZATIONS FOR THE MODEL IN DIFFERENT DETECTORS

Detector Name	Off-Eclipse	Primary Eclipse	Secondary Eclipse
SIS0, 1	1.0(f)	1.0(f)	1.0(f)
GIS2, 3	$0.82^{+0.01}_{-0.01}$	$0.81^{+0.02}_{-0.03}$	$0.81^{+0.02}_{-0.02}$

NOTE.—Errors and upper limits are with 90% confidence based on $\chi^2_{min} + 2.71$; f means frozen value.

3.3. *Errors on Abundance Measurements*

The errors quoted in the tables and the text of the paper are statistical errors and should be regarded as lower limits. The systematic errors in the underlying atomic physics of the plasma code are much more open to debate. The spectrum emitted by a typical stellar corona in the 0.5–10 keV region is strongly influenced by the Fe plasma. Thus, when we fit an observed coronal spectrum with a "meka" model spectrum, it is T_e and f_{Fe} EM, where f_{Fe} is the Fe abundance relative to its solar photospheric value that are the most well determined of the parameters, and the absolute values of f_{Fe} and the other elemental abundances are more loosely constrained. This also results in better constraints for the abundances of the heavy elements relative to Fe than their abundances relative to hydrogen.

It should be understood further that the formal fit errors apply to an ideal world in which it is implicitly assumed that

(*a*) the models used are exact representations of real thermal plasmas, (*b*) the response of the X-ray detector and telescope to X-rays is perfectly characterized by the response matrix that has been used in the analysis, and (*c*) other effects such as background subtraction and corrections resulting from gain variations have all been done correctly. In the real world, however, none of these assumptions are true, although the formal errors do, in principle, include contributions from type (*c*) effects. The largest source of error that is not included in the formal fit errors is that associated with type (*a*), and it is particularly acute for the Fe-L shell region of 0.7–1.4 keV: it is known that the "meka" code used in the present analysis can over- or underestimate individual lines by as much as factors of 2 or 3 (Liedahl et al. 1995). Until the next-generation plasma code is available for comparison, it is impossible for us to say how the problems with the current "meka" code will affect the inferred Fe abundance and that of other elements with strong line emission. According to Liedahl et al. (1995), some lines are underestimated, while other lines are overestimated. But, as we have explicitly demonstrated, a similar Fe underabundance is inferred if we exclude the Fe-L shell region from the analysis and determine the Fe abundance only from the strength of the 6.7 keV Fe XXV feature.

The same discussion applies to the other elements. The most reliable abundances are for those elements which have strong, isolated, and clearly resolved lines or line complexes in the *ASCA* spectral range. Listing the elements in order of decreasing reliability, the abundances of Si, S, O, Ca, and Ar should be relatively robust while Mg, Ni, Ne, and N should be considered more suspect:

1. The factor of 2 underabundance of Si is determined predominantly from the Si XIII/XIV complex at 1.9 keV: this feature is strong and should not suffer from significant contamination from other species, and the atomic physics of these H- and He-like ions should be accurately known.
2. The factor of 4–5 underabundance of S is robust because it is based mostly on the observed strength of the He- and H-like S XV/XVI complex at 2.5 keV. This feature is predicted to be strong in solar abundance coronal plasmas of the temperatures that prevail in AR Lac's corona, but it is only marginally detected in the *ASCA* spectrum.
3. The factor of 2–3 underabundance of O is derived mostly from the observed strength of the O VIII line at 0.65 keV: this feature is not seen as an individual line in *ASCA* SIS spectra but is blended with the low-energy edge of the Fe-L shell complex which is predicted for these temperatures to be at $\sim$0.73 keV. This makes the abundance determination of O less reliable, although if the abundance were solar it would result in a strong feature which is not seen.
4. The Ca underabundance is based mostly on the He-like and H-like Ca XIX/XX feature at 4.0 keV (a relatively unconfused region) that would have been observed if the plasma had solar abundances. Although relatively weak in emissivity compared to the previous lines discussed, its absence in the observed spectrum of AR Lac is significant, and hence the tabulated upper limit should be robust.
5. The factor of 2–3 underabundance of Ar is based primarily on the H-like Ar XVIII line that is predicted to be at 3.3 keV, but which is observed at no more than one-third of its predicted strength in a solar abundance plasma. Similarly to the Ca resonance line, the Ar line is in a relatively unconfused spectral region, and thus its low estimated abundance seems secure.
6. The Mg abundance is based on the observed strength of the He- and H-like Mg XI/XII complex at 1.4 keV: this feature is also predicted to be one of the most distinguishable ones present in coronal plasmas, and indeed it usually is. It does suffer from confusion caused by lines of other species, primarily Ni and Fe lines, particularly for plasmas with temperatures $\geq$1 keV, and this line may be compensating for the uncertainties in the Fe-L emission.
7. The strongest predicted lines of Ne and Ni are either in the middle of the Fe-L complex at 0.9–1.0 keV or are confused with the Mg XI/XII and Fe complex at 1.4 keV. The previously discussed model uncertainties of the Fe-L lines can produce large systematic errors in the derived Ne and Ni abundances that are probably much larger than the formal fit errors given in the tables. Thus, these abundances should be considered as very uncertain.
8. The absence of N in the spectrum of AR Lac is inferred from the absence of any obvious line attributable to N VII at 0.50 keV, which feature is predicted to be strong in solar abundance plasmas (and whose atomic physics is known very accurately). To our knowledge, no SIS spectrum of any star has shown evidence for this feature, implying either an absence of N in stellar coronae, or that the effective area of the SISs at this energy has been overestimated by a factor of 10 or more. The line lies close to the low-energy cutoff and hence in a spectral region where the effective area is rapidly decreasing toward shorter energies. The CCD detectors have a layer of silicon nitride, and uncertainties in modeling its effects in the spectral response function could also be responsible.

3.4. *Primary and Secondary Eclipse Spectra*

The spectral data obtained from four detectors (SIS0, SIS1, GIS2, and GIS3) were analyzed jointly, for the off-eclipse phases, and during the primary and secondary eclipses. The relative normalization for the GIS detectors as compared to the SIS detectors was kept as a free parameter. The off-eclipse phase spectra were fitted first, and the abundances determined from this analysis were used as frozen values for the subsequent analysis of the eclipse spectra because of the poorer statistics of the short duration eclipse spectra. The N_H was fixed at the highest value, viz., 4.4×10^{18} cm^{-2}, allowed by the 2T fit to the combined *ROSAT* and *ASCA* data (§ 3.2.1). The SIS detectors are insensitive to the values of N_H in this range. The results from this analysis based on the two-temperature "meka" plasma are given in Table 4. No significant changes are found compared to the analysis presented in the previous section (compare with Table 1). The temperatures were found to remain unchanged during the eclipse, and the relative normalizations were found to require the same correction to the current GIS response matrices. The relative emission measure (EM) values of the low- and high-temperature components do change during the primary eclipse (see Table 4). The EM of the low-temperature component decreases by at least 35% (the eclipse spectra are averaged over the true minimum) compared to that of the high-temperature component, which appears to decrease by $\geq$45%. A similar difference in the change of EM values of the 2T components is not ruled out during the secondary minimum but is difficult to infer from the present data because the depth of the secondary minimum is only about 15% and the uncertainty in the EM is about 5%.

4. DISCUSSION

Plasma emission models with solar photospheric abundances, and having two, three, or four discrete temperature

components or continuously distributed emission measure as a function of temperature, are found to give poor fits relative to variable abundance models in fitting the X-ray spectra of AR Lac. This result is unchanged even if the Fe-L region (0.7–1.7 keV), in which the presently available plasma code is most uncertain (Liedahl et al. 1995), is excluded from the fit. Our results show that the existing X-ray spectra are more sensitive to the determination of elemental abundances than to the underlying distribution of emission measure as a function of temperature. The 2T model with variable abundances provides a marginally better fit to the X-ray spectra than the variable abundance CEM models. Dempsey et al. (1993), using PSPC observations of RS CVn binaries, and Lemen et al. (1989), based on high-resolution data (*EXOSAT* Transmission Grating) of Capella, Procyon, and an RS CVn binary (σ^2 CrB), have also argued in favor of a discrete 2T model. According to Lemen et al. (1989), the discrete components represent the distinct ensembles of static loops with different maximum temperatures and expansions of the loop cross section from the footpoint to the apex. The solar flare plasma shows a bimodal temperature distribution with the two different temperatures, the "quasi-hot," 0.4–0.7 keV, and "hot," 1.4–2.2 keV, plasmas, where the hotter component is present only during the flares (Antonucci & Dodero 1995). The two components probably have a common origin in the flaring regions on the Sun, since the "quasi-hot" component cools to active region temperatures of 0.2–0.3 keV during the flare decay (Antonucci & Dodero 1995). The temperatures of the two components are remarkably close to the temperatures found in the X-ray emission from RS CVns.

Spectral analysis during the primary and secondary eclipses shows that the emission measure of the high-temperature component in the 2T model appears to be more affected by the primary eclipse than the low-temperature component. This suggests that a larger amount of emission corresponding to the high-T component is concentrated in structures that are spatially more compact than the emission corresponding to the low-temperature component. The same result is derived independently from a detailed analysis of the *ASCA* light curves by Siarkowski et al. (1995).

The abundance of Fe in the corona of AR Lac is determined to lie in the range of 0.14–0.53 the solar photospheric value. The same value is derived based on simple two-temperature models as well as the more complex CEM models. The derived abundances of O, Si, S, Ar, and Ca are independent of the uncertainties in the plasma codes in the Fe-L region and should be reliable. In contrast, the Ne and Mg abundances are quite uncertain because these lines overlap the Fe-L region. Higher spectral resolution is required to deconvolve these lines.

Prior to *ASCA*, observations with *Ginga* of a small number of active stars (e.g., UX Ari [Tsuru et al. 1989], II Peg [Doyle et al. 1991], Algol [Stern et al. 1992], and AB Dor [Vilhu, Tsuru, & Collier Cameron 1991]) showed that there was a deficiency by a factor of 2 or 3 of the observed emission from the Fe XXV line at 6.7 keV compared to that predicted by the solar abundance coronal plasma models. This observed weakness in *Ginga* Large Area Counter spectra of active stars is roughly consistent with the Fe underabundances inferred from *ASCA* spectra of such stars which are based on the observed strengths of the Fe-L (primarily) and Fe XXV complexes relative to those of the 0.5–10 keV continuum. An alternative explanation for the weakness of the 6.7 keV emission is that the Fe abundance is normal and it is optical depth effects that reduce the flux in the Fe XXV resonance line by resonant scattering of line photons out of the line of sight. This hypothesis has been discussed by Tsuru et al. (1989). We estimate the effects of the optical depth on the resonance lines of the He-like ions of Fe, Si, and Mg based on the discussion of Tsuru et al. and that of Acton (1978), who discussed the optical depth effects in solar coronal resonance lines. Assuming a solar (photospheric) Fe abundance of 4.68×10^{-5} (Anders & Grevesse 1989), we have for the line center opacity of the Fe XXV resonance line:

$$\kappa_0 = 9.9 \times 10^{-22} A_i N_e (T_e/2 \text{ keV})^{-0.5} ,$$

where A_i is the fraction of Fe that is Fe XXV. We shall assume that $T_e = 2$ keV, the temperature of the hot component inferred from our previous analysis based on a simple 2T model (the cool plasma component essentially produces no Fe XXV emission and can be ignored in the present context). For 2 keV, Arnaud & Rothenflug (1985) predict that 74% of Fe is Fe XXV, and hence we obtain for the optical depth τ_0 of the Fe XXV line

$$\tau_0 = C_{\text{ion}} N_e l ,$$

where $C_{\text{ion}} = 7.0 \times 10^{-22}$ and l is the column length of the emitting plasma. Thus, given the electron density and column length of the emitting plasma, we can estimate τ_0. Independent estimates of the electron densities prevailing in RS CVn coronae can be obtained from, for example, the observed decay times of X-ray flares (e.g., Doyle et al. 1991; Jeffries & Bedford 1990; Tagliaferri et al. 1991; Ottmann & Schmitt 1994) and typically range from 10^{10} to 10^{12} cm^{-3}. One might expect that the electron density of the nonflaring coronae in such systems is somewhat less than that prevailing during a large flare, and thus we will adopt a plausible range from 10^{10} to 3×10^{11} cm^{-3} for the "typical" coronal electron density in AR Lac. An additional constraint can be obtained if we argue that, given the eclipses observed in the X-ray region for AR Lac, the column length of the hot component is no larger, and probably much smaller, than the radius of either of the component stars. Finally, we consider two possible geometries of the emission regions, the first that the emission comes from spherical shells around both stars of thickness h so that $V = 2\pi(R_1^2 + R_2^2)h$, and the second that the emission comes a discrete number f of (for simplicity) cubic regions of linear dimension L so that $V = fL^3$. In the first case, it can easily be shown that using EM $= 6.25 \times 10^{53}$ cm^{-3}, as given in Table 1, implies that $\tau_0 = 1.5 \times 10^9 N_e^{-1}$. Thus, for all plausible values of the electron density the optical depth is always $\ll 1$. In the second case, we obtain $\tau_0 = 6.3 \times 10^{-4}(N_e/f)^{1/3}$, implying that the fewer the discrete regions, the larger the optical depth. For example, if $f = 1$, then $\tau_0 \sim 1.4$–4.2 for the range of electron densities considered, while if $f = 10$, perhaps a more realistic assumption, then $\tau_0 \sim 0.6$–1.9.

The optical depth of the Fe XXV resonance line in the corona of AR Lac is constrained only to be less than a few (but might indeed be negligible), so that in fact we cannot rule out the possibility that its strength is less than that which would be produced by an optically thin plasma. In fact, the Fe "line" at 6.70 keV produced by a 2 keV temperature plasma is (at the spectral resolution of *ASCA*) a blend of the Fe XXV resonance line and a number of other lines, primarily Fe XXV intercombination and forbidden lines at 6.67 and 6.63 keV, respectively, and the Fe XXIV Li-like lines at 6.70, 6.69, and 6.65 keV. Using the Mewe et al. (1985) tabulation of line powers, we estimate that the resonance line is contributing only 27% of the total power in this complex, so that even if it were completely

suppressed, the observed strength of this whole feature would only be decreased by this same amount. Thus, we concur with the conclusion of Tsuru et al. (1989) that resonant scattering of Fe XXV photons does not seem to be able to explain the observed weakness of the Fe K complex in the coronal spectra of RS CVn stars.

We have done similar calculations for the Si XIII 1.86 keV line and the Mg XI 1.35 keV line, for which C_{ion} is 3.1×10^{-21} and 2.5×10^{-21}, respectively (i.e., these values are about 4 times larger than the corresponding value for Fe XXV). To calculate C_{ion} for the Si and Mg lines, we have assumed that they are formed at the temperature of 0.6 keV typical of the lower temperature component in Table 1 which has an emission measure of 4.1×10^{53} cm^{-3}. Using similar geometrical models as before for the Fe XXV optical depth, we estimate that the optical depths of the He-like Si and Mg resonance lines could range from negligible up to ~ 10.

Thus, we believe that optical depth effects are not negligible for X-ray lines formed in stellar coronae. However, it is unlikely that optical depths of a few produce any observable effects in X-ray spectra with spectral resolution in excess of ~ 10 eV. Resonant scattering does not destroy line photons per se but merely redistributes them in energy and/or direction. Resonant scattering can, however, indirectly lead to the "loss" of line photons. Schrijver, van den Oord, & Mewe (1994) show that in the context of stellar coronal EUV lines, if there is an asymmetry in the relative distribution of emitting and scattering regions, some geometries will result in more photons being scattered back into the stellar photosphere (where they are destroyed) than are scattered outward toward the observer. In extreme cases, this might lead to the destruction of as many as half the resonance line photons, but for more realistic geometries this will almost certainly be a much smaller effect. Again, however, since the resonance lines are predicted to typically contribute only 25%–50% of the total emission in the entire line complexes for these ions even if 50% of the resonance line photons are lost, the decrease in the strength of the whole line complex will be only 12%–25%. We conclude that optical depth even in its most extreme form cannot produce the typical factor of 2–4 line weakening that we have inferred in the present analysis of the coronal spectrum of AR Lac.

5. CONCLUSIONS

To summarize, our analysis of the *ROSAT* and *ASCA* spectra of AR Lac leads to the following conclusions:

1. Two-temperature component models with variable abundance provide the best fit to the simultaneously obtained *ASCA* and *ROSAT* X-ray spectra of AR Lac. This result holds even when the Fe-L region is excluded from the fit.
2. Solar abundance CEM models, representing static solar coronal loops, are ruled out. Variable abundance CEM models provide a marginally acceptable fit but are still not as good as the 2T model with variable abundance.
3. Based on a simple 2T model, a larger fraction of the high-temperature component is eclipsed, suggesting that a larger fraction of this component is concentrated in structures that are spatially more compact.
4. Abundances typically 0.2–0.5 the solar photospheric value are required for O, Si, S, Ar, Ca, and Fe irrespective of the temperature distribution model used to fit the X-ray spectra.
5. Opacity effects in the Fe XXV resonance line are not likely to be the cause of reduced emission seen in this line when compared to that expected from solar photospheric abundance of Fe.

We thank Peter Serlemitsos and Tahir Yaqoob for making the initial *ROSAT* proposal and arranging the simultaneous observations. We thank Y. Tanaka and the entire *ASCA* team for making the observation possible.

REFERENCES

Acton, L. W. 1978, ApJ, 225, 1069
Anders, E., & Grevesse, N. 1989, Geochim. Cosmochim. Acta, 53, 197
Antiochos, S. K., & Noci, G. 1986, ApJ, 301, 440
Antonucci, E., & Dodero, M. A. 1995, 438, 480
Antunes, A., Nagase, F., & White, N. E. 1994, ApJ, 436, L83
Arnaud, M., & Rothenflug, R. 1985, A&AS, 60, 425
Burke, B. E., Mountain, R. W., Harrison, D. C., Bautz, M. W., Doty, J. P., Ricker, G. R., & Daniels, P. J. 1991, IEEE Trans., ED-38, 1069
Craig, J. D., & Brown, J. C., A&A, 49, 239
Dempsey, R. C., Linsky, J. L., Schmitt, J. H. M. M., & Fleming, T. A. 1993, ApJ, 413, 333
Diplas, A., & Savage, B. D. 1994, ApJS, 93, 211
Doyle, J. G., et al. 1991, MNRAS, 248, 503
Drake, S. A., Singh, K. P., White, N. E., & Simon, T. 1994, ApJ, 436, L87
Fruscione, A., Hawkins, I., Jelinsky, P., & Wiercigroch, A. 1994, ApJS, 94, 127
Gehrels, N., & Williams, E. D. 1993, ApJ, 418, L25
Grevesse, N., Noels, A., & Sauval, A. J. 1992, in Proc. First SOHO Workshop (ESA SP-348) (Noordwijk: ESA Publications Division, ESTEC), 305
Hall, D. S. 1976, in IAU Colloq. 29, Multiply Periodic Phenomena in Variable Stars, ed. W. S. Fitch (Dordrecht: Reidel), 287
Jeffries, R. D., & Bedford, D. K. 1990, MNRAS, 246, 337
Kaastra, J. S. 1992, An X-Ray Spectral Code for Optically Thin Plasmas (SRON-Leiden Report, updated version 2.0)
Lemen, J. R., Mewe, R., Schrijver, C. J., & Fludra, A. 1989, ApJ, 341, 474
Liedahl, D. A., Osterheld, A. L., & Goldstein, W. H. 1995, ApJ, 438, L115
Majer, P., Schmitt, J. H. M. M., Golub,L., Harnden, F. R., Jr., & Rosner, R. 1986, ApJ, 300, 360
Mewe, R., Gronenschild, E. H. B. M., & van den Oord, G. H. J. 1985, A&A, 62, 197
Ohashi, T., Makishima, K., Ishida, M., Tsuru, T., Tashiro, M., Mihara, T., Kohmura, Y., & Inoue, H. 1991, Proc. SPIE, 1549, 9
Ottmann, R. 1993, A&A, 273, 546
Ottmann, R., & Schmitt, J. H. M. M. 1994, A&A, 283, 871
Ottmann, R., Schmitt, J. H. M. M., & Kurster, M. 1993, ApJ, 413, 710
Pfeffermann, E., et al. 1987, Proc. SPIE Int. Soc. Opt. Eng., 733, 519
Raymond, J. C. 1990, private communication
Raymond, J. C., & Smith, B. W. 1977, ApJS, 35, 419
Schmitt, J. H. M. M., Collura, A., Sciortino, S., Vaiana, G. S., Harnden, F. R., Jr., & Rosner, R. 1990, ApJ, 365, 704
Schrijver, C. J., van den Oord, G. H. J., & Mewe, R. 1994, A&A, 289, L23
Serlemitsos, P. J., et al. 1995, PASJ, 47, 105
Siarkowski, M., Pres, P, White, N. E., Singh, K. P., & Drake, S. A. 1995, ApJ, submitted
Singh, K. P., Drake, S. A., & White, N. E. 1995, ApJ, 445, 840
Stern, R. A., Antiochos, S. K., & Harnden, F. R. 1986, ApJ, 305, 417
Stern, R. A., Lemen, J. R., Schmitt, J. H. M. M, & Pye, J. P. 1995, ApJ, 444, L45
Stern, R. A., Uchida, Y., Tsuneta, S., & Nagase, F. 1992, ApJ, 400, 321
Swank, J. H., White, N. E., Holt, S. S., & Becker, R. H. 1981, ApJ, 246, 208
Swartz, D. A., O'Dell, S. L., Sulkanen, M. E., & Tennant, A. F., Jr. 1994, ApJ, L149
Tagliaferri, G., White, N. E., Doyle, J. G., Culhane, J. L., Hassall, B. J. M., & Swank, J. H. 1991, A&A, 251, 161
Tanaka, Y., Inoue, H., & Holt, S. S. 1994, PASJ, 46, L37
Trümper, J. 1983, Adv. Space Res., 2, 241
Tsuru, T., et al. 1989, PASJ, 41, 679
Turner, T. J., & George, I. M. 1994, ROSAT PSPC Calibration Guide (Documentation available at US ROSAT Science Data Center & HEASARC)
Vesecky, J. F., Antiochos, S. K., & Underwood, J. H. 1979, ApJ, 233, 987
Vilhu, O., Tsuru, T., & Collier Cameron, A. 1991, in Iron Line Diagnostics in X-Ray Sources, ed. A. Treves, G. C. Perola, & L. Stella (Berlin: Springer-Verlag), 30
White, N. E., Arnaud, K., Day, C. S. R., Ebisawa, K., Gotthelf, E., Mukai, K., Soong, Y., Yaqoob, T., & Antunes, A. 1994, PASJ, 46, L97

Note added in proof.—After the paper was accepted, the revised coronal plasma emission code "mekal," named after its principal authors (R. Mewe, J. S. Kaastra, & D. A. Liedahl, Legacy, 6, 16 [1995]), became available. We have fitted the data using the latest version of this code and find that the abundances of Ne, Mg, Si, S, Ar, Ca, and Fe are lower by $\sim 20\%$, and that of O is lower by $\sim 60\%$ compared to the values quoted in Table 1. The temperatures are essentially unaffected.